Hindawi
Mathematical Problems in Engineering
Volume 2022, Article ID 9319190, 21 pages
https://doi.org/10.1155/2022/9319190

*Research Article*

# Seismic Response Analysis of Isolated and Nonisolated Continuous Girder Bridges under Multidimensional Near-Field Ground Motions

**Ying Gao**,[1] **Xiaoyu Yan**,[2] **Junjie Chen**,[1] **Liang Zheng**,[1] **and Yunshan Han**[1]

[1]*School of Science, North University of China, Taiyuan 030051, China*
[2]*School of Engineering, The Open University of China, Beijing 100039, China*

Correspondence should be addressed to Ying Gao; gaoying@nuc.edu.cn

Received 20 March 2022; Accepted 17 May 2022; Published 6 June 2022

Academic Editor: Linsheng Huo



In this study, the responses of isolated bridges and nonisolated bridges are studied under multidimensional seismic motions. First, damage constitutive models of steel bars and concrete materials were combined with the fiber beam-column element model, and the isolated bearing model considering bearing failure was selected. The bridge numerical analysis model was then established. The seismic responses of isolated and nonisolated bridges were analyzed under near-field ground motions (fling-step and forward-directivity ground motions) and far-field ground motions. It was found that the seismic responses of nonisolated bridges, such as deck acceleration, pier displacement, pier damage, and bearing displacement under near-field ground motions, were higher than those under far-field ground motions. Under far-field ground motions, isolation bearings effectively reduced various seismic responses of structures and had isolation effects. Under forward-directivity TCU102 ground motions, the minimum isolation ratios of isolation bearings for peak acceleration of the girder in the $Z$ direction, pier displacement, and pier shear force were −0.14, −2.65, and −0.05, respectively. The low-isolation ratio and significant damage to the isolation bearings indicate that the isolation bearings cannot be directly used under near-field conditions.

## 1. Introduction

There have been numerous fault ruptures in high-density urban areas, such as the 1994 Northridge earthquake in the United States, the 1995 Kobe earthquake in Japan, the 1999 Kocaeli earthquake in Turkey, the 1999 Chi-Chi earthquake in Taiwan, and the 2008 Wenchuan earthquake in Sichuan. These earthquakes caused extensive building and bridge damage throughout the cities. The concentration of earthquake damage is reflected in the extreme earthquake area, enlisting the need for further study and development of better engineering practice. Near-field motion characteristics [1] mainly include forward-directivity, fling-step, hanging-wall, and significant vertical ground motion. Among them, the forward-directivity effect is one of the main reasons causing the characteristics of near-field ground motions' pulse, which is caused by the Doppler effect of fault rupture propagation and shows a bidirectional velocity pulse [2]. The fling-step effect is when the two plates of the fault are relatively dislocated or slide during an earthquake, and finally, permanent ground displacement is generated in the sliding direction [3]. The velocity pulse caused by the fling-step effect is related to the magnitude of permanent displacement and the timing of permanent displacement, which is a unidirectional pulse. Peak pulse velocity has a significant influence on structural demands [4, 5]. Velocity pulse is one of the leading causes of near-field structure failure. Under near-field pulse-like ground motions, the effectiveness and applicability of isolation technology need to be studied and globally implemented [1].

Bridge isolation technology has been widely used in the seismic design of bridges. However, when designing and analyzing isolated bridges, the influence of near-field ground motions on the seismic responses of bridges is often ignored.

With the in-depth study of near-field ground motions, the characteristics, laws, and potential failure mechanism of seismic response of isolated bridges under near-field ground motions have gradually become the focus of research. Jonsson et al. [6] analyzed the response of an isolated bridge under strong near-field ground motions and found that a practical design of an isolation system can effectively prevent the bridge structure from damage. Wei et al. [7] analyzed the seismic response of an isolated, simply supported girder bridge and found that the isolated bearing still has some seismic absorption effect under near-field ground motions. Jalali et al. [8, 9] analyzed the response of a three-span bridge with mid-span isolation under near-field pulse-like ground motion. They studied the difference between parallel fault and vertical fault ground motion to the structural response. Ismail et al. [10] analyzed and studied the isolation effect of a new type of roll-in-cage (RNC) isolator under near-field, long-period, and pulse-like ground motions and verified the effectiveness of the isolation bearing. Losanno et al. [11] optimized the damping parameters of isolated bridges through numerical simulation and compared the influence of near-field and far-field ground motions on isolation effects. Liao et al. [12] found that the PGV/PGA ratio of near-field ground motion greatly influences the bridge response. Kalkan and Kunnath [13] studied the effect of forward directivity and fling step on the seismic response of steel frame structures. Zheng et al. [14] analyzed the seismic performance of bridges installed with a sliding-lead rubber-bearing isolation system subjected to near-fault earthquakes. Jiang et al. [15] proposed a risk-based approach to study the pulse effect on the isolator optimization of bridges in near-fault zones. In the study of isolated bridges, the influence of forward directivity and fling step on bridge response is seldom distinguished. In addition, most studies only consider unidirectional or bidirectional ground motion, but not three-dimensional ground motion.

At present, the failure of isolated bearings is not considered in the seismic response research of most isolated bridges, or only the critical displacement is used to judge if the bearings are damaged, which is unsafe. Buckle et al. [16] found that the critical load value of the bearing decreases with the increase in lateral displacement through experimental research. It is essential to consider the change in critical load when designing bearings. Li et al. [17] proposed a three-dimensional isolation bearing simulation model that considers the horizontal bidirectional coupling effect and vertical stability, which can better simulate the nonlinear mechanical characteristics and vertical stability of isolation bearings.

The research on isolated bridges typically does not focus on pier damage because the isolated bearings can better protect the safety of piers under far-field ground motions, and the piers are basically in an elastic state with minor damage. However, under near-field ground motions, piers may be damaged. Zhong et al. [18] proposed an uncoupled multivariate power model to estimate the performance-based seismic damage states of column curvature ductility. The fiber-element model with computational efficiency and numerical accuracy is suitable for the nonlinear analysis of reinforced concrete members [19]. Heo and Kunnath [20] proposed a damage model of reinforced concrete members based on material damage using the fiber-element model. The model takes the damage indexes of the critical fibers of compressed concrete and the critical fibers of reinforcement in the core area of concrete as the cross-sectional damage indexes. Li et al. [21] and Gao et al. [22] used the fiber-element model combined with the Faria-Oliver uniaxial concrete damage model [23] to analyze the damage to reinforced concrete members.

In this study, based on the refined simulation and analysis platform for structures (RSAPS) [24] previously developed, the fiber beam-column element model and the three-dimensional isolation bearing model [17] are used to simulate the nonlinear characteristics of piers and isolation bearings, respectively. The concrete damage constitutive model [25] and the steel bar constitutive model [25] were combined with the fiber beam-column element, establishing the damage analysis model of the reinforced concrete bridge. Three-dimensional near-field ground motions (fling-step and forward-directivity ground motions) and far-field ground motions were selected to analyze the seismic response of isolated bridges and nonisolated bridges, respectively.

## 2. Ground Motion Record Selection

According to the research results of Kalkan and Kunnath [13], Sehhati et al. [26], Moniri [27], Li et al. [28], and Wang and Bai [29], seven forward-directivity ground motions, seven fling-step ground motions, and seven far-field ground motions were obtained from the Pacific Earthquake Engineering Research Center database [30]. The selected ground motion records and their parameters are shown in Tables 1–3.

## 3. Finite Element Model of Reinforced Concrete Bridge

In this study, the simulation analysis platform RSAPS [24] was used to simulate and analyze the seismic response of reinforced concrete bridges. The RSAPS platform was established based on the subroutine (UEL) interface of the general finite element software ABAQUS and mainly included the fiber beam-column element model, isolation element model, and various material constitutive models of concrete and steel. Good simulation results [24] have been achieved for static and dynamic nonlinear behavior simulation of reinforced concrete members. The specific bridge model is given below.

*3.1. Analysis Model of the Bridge.* The seismic response analysis of a bridge (Figure 1) in reference [24] was carried out. The bridge is a continuous girder bridge with a span of 30 m and five spans. The girder has a single-box and three-chamber section with a height of 1.88 m and a width of 8.025 m. The pier height is 6.6 m, and the diameter is

Table 1: Near-field ground motion records (fling step) and parameters.

| Number | Earthquake | Station | Mw | PGAx(g) | PGAy(g) | PGAz(g) | Site class |
|---|---|---|---|---|---|---|---|
| TCU054 | Chi-chi | TCU054 | 7.6 | 0.19 | 0.15 | 0.14 | C |
| TCU065 | Chi-chi | TCU065 | 7.6 | 0.79 | 0.58 | 0.26 | D |
| TCU068 | Chi-chi | TCU068 | 7.6 | 0.51 | 0.37 | 0.53 | C |
| TCU072 | Chi-chi | TCU072 | 7.6 | 0.48 | 0.38 | 0.28 | C |
| TCU076 | Chi-chi | TCU076 | 7.6 | 0.34 | 0.43 | 0.28 | C |
| TCU082 | Chi-chi | TCU082 | 7.6 | 0.23 | 0.19 | 0.13 | C |
| Yarimca | Kocaeli | Yarimca | 7.5 | 0.23 | 0.32 | 0.24 | D |

Table 2: Near-field ground motion records (forward directivity) and parameters.

| Number | Earthquake | Station | Mw | PGAx(g) | PGAy(g) | PGAz(g) | Site class |
|---|---|---|---|---|---|---|---|
| Duzce | Kocaeli | Duzce | 7.5 | 0.31 | 0.36 | 0.21 | D |
| JFPA Building | Northridge | Jensen-FPAB | 6.7 | 0.41 | 0.62 | 0.35 | C |
| Lexington Dam | Loma Prieta | Lexington Dam | 6.9 | 0.44 | 0.41 | 0.14 | B |
| SCSE | Northridge | Sylmar-CSE | 6.7 | 0.85 | 0.45 | 0.48 | C |
| SOVMFF | Northridge | Sylmar OVMFF | 6.7 | 0.60 | 0.84 | 0.54 | C |
| TCU101 | Chi-Chi | TCU101 | 7.6 | 0.21 | 0.26 | 0.17 | C |
| TCU 102 | Chi-Chi | TCU 102 | 7.6 | 0.30 | 0.17 | 0.18 | C |

Table 3: Far-field ground motion records and parameters.

| Number | Earthquake | Station | Mw | PGAx(g) | PGAy(g) | PGAz(g) | Site class |
|---|---|---|---|---|---|---|---|
| Abbar | Manjil, Iran | Abbar | 7.4 | 0.51 | 0.50 | 0.54 | C |
| AnzaTule | N. Palm Springs | Anza-Tule Canyon | 6.1 | 0.10 | 0.10 | 0.04 | C |
| BakerFire | Landers | Baker Fire Station | 7.3 | 0.11 | 0.11 | 0.06 | D |
| BigBear | Big Bear-01 | Desert Hot Springs | 6.5 | 0.23 | 0.18 | 0.12 | D |
| Calexico | Imperial Valley | Calexico Fire Station | 6.5 | 0.28 | 0.20 | 0.19 | D |
| LaCCNth | Northridge | LA-Century City CC North | 6.7 | 0.26 | 0.22 | 0.12 | D |
| Yarimca | Kocaeli | Yarimca | 7.5 | 0.23 | 0.32 | 0.24 | D |

1.219 m. The section of the girder and the pier is shown in Figure 2.

In modeling analysis, because the main bridge girders are mostly prestressed reinforced concrete structures, the girders seldom undergo plastic deformation or damage behavior when subjected to an earthquake. The linear elastic beam element was used to simulate the girders, and each span was divided into 15 elastic beam elements. The pier was the primary stress member; strong nonlinear behaviors such as plasticity and damage appear during an earthquake; and they were simulated using the fiber beam-column elements.

For the isolated bridge in reference [24], LRB700-140 isolation bearings were selected. The bearing diameter is 700 mm, the lead diameter is 140 mm, the total thickness of the rubber layer is 110 mm, and the total thickness of the steel plate layer is 75 mm. The preyield stiffness of the bearing is 17.771 kN/mm, the postyield stiffness is 1.367 kN/mm, and the yield force is 94.2 kN. The critical design load is 4618 kN. The LRB bearings were simulated by isolation elements (shown in Section 3.3).

To study the isolation effect of LRB isolation bearings, the bearings in the nonisolated bridge model were assumed to be ordinary linear elastic bearings, and the stiffness of the bearings was taken as the preyield stiffness of LRB bearings at corresponding positions in the isolated bridges [24]. The bearings in nonisolated bridges were simulated as spring elements.

*3.2. Pier Analysis Model.* The fiber beam-column element was adopted for modeling the nonlinear behavior of a pier. Each member was divided into six fiber beam-column elements along with the height. Each element adopts four Gauss-Lobatto integral sections. Each section was divided into 48 longitudinal reinforcements and 216 concrete fibers, including 180 core and 36 protective layer concrete fibers. The cross-sectional fiber discretization method is shown in Figure 3.

*3.2.1. Constitutive Model for Concrete Material.* Yassin's uniaxial concrete model [31] was implemented in this study (as shown in Figure 4). Yassin's model has the following advantages: (1) this model can simulate the continuous stiffness degradation effect during unloading and reloading with an increase in concrete compressive strain; (2) under repeated loading and unloading, the hysteretic performance of concrete materials can be effectively simulated. The model can also simulate the stirrup constraint effect by modifying the characteristic parameters of the concrete materials.

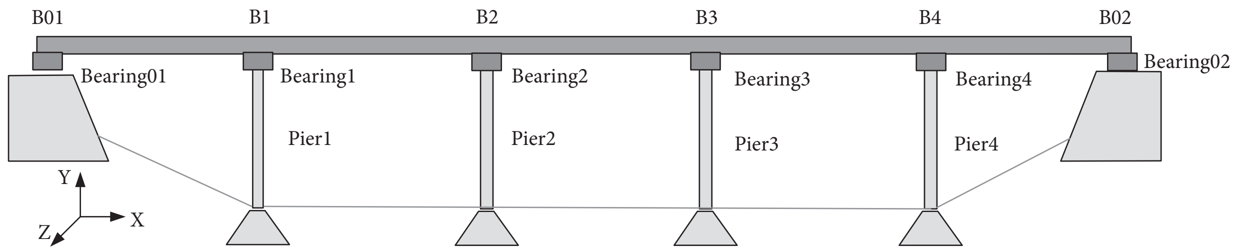


Figure 1: Analysis model of the bridge.

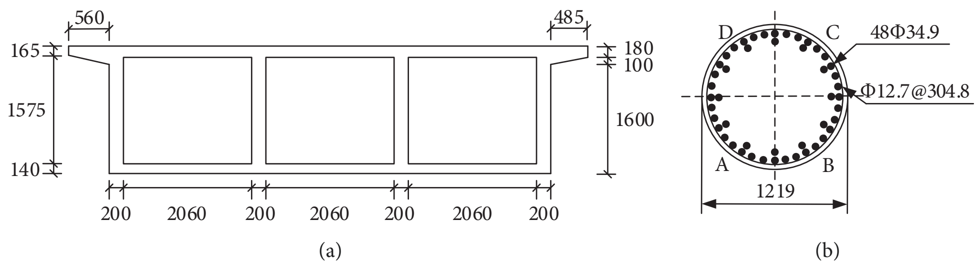


Figure 2: The section of the girder and the pier. (a) The section of the girder. (b) The section of the pier.

To consider the damage performance in the uniaxial constitutive model of concrete, the tensile and compressive damage indexes of concrete are used to describe the tensile and compressive damage of concrete, respectively. The damage distribution and its evolution process can be intuitively described.

*(1) Compression Damage*. According to the basic principle of damage mechanics and the characteristics of the concrete constitutive model, the calculation method of compression damage index is as follows [25]:

$$D_c = \begin{cases} 0, & \varepsilon_{cm}^{c} < \varepsilon_{c\ d0}^{c}, \\ \dfrac{E_{c\ d0} - E_{cm}}{E_{c\ d0} - E_{c20}}, & \varepsilon_{c\ d0}^{c} \le \varepsilon_{cm}^{c} \le \varepsilon_{20}, \\ 1, & \varepsilon_{20} < \varepsilon_{cm}^{c}, \end{cases} \tag{1}$$

where $D_c$ is the compression damage index of concrete; $E_{c\ d0} = (\sigma_{c\ d0}^{c} - \sigma_r)/(\varepsilon_{c\ d0}^{c} - \varepsilon_r)$ is the initial compression damage module, determined according to the compression damage starting point $D_0(\varepsilon_{c\ d0}^{c}, \sigma_{c\ d0}^{c})$ and the focus $R(\varepsilon_r, \sigma_r)$; and $E_{cm} = (\sigma_{cm}^{c} - \sigma_r)/(\varepsilon_{cm}^{c} - \varepsilon_r)$ is the module of the current unloading point, determined according to the unloading point $D(\varepsilon_{cm}^{c}, \sigma_{cm}^{c})$ and the focus $R(\varepsilon_r, \sigma_r)$.

Compression damage of concrete only occurs during loading but does not occur during unloading. New damage occurs only after reloading reaches the previous unloading point. According to Yue et al.'s research [32], a point when stress in the rising section of the skeleton curve reaches 0.3 $f_c'$ is selected as the damage starting point. The stress-strain relationship and corresponding compression damage index of concrete under compression are shown in Figure 5.

For the convenience of expression and understanding, the stress is placed in the first quadrant in the introduction of the compression characteristics of the above concrete, and the principle of positive tension and negative compression is followed in practical application.

*(2) Tensile Properties*. A linear model was adopted for the stress-strain relationship curve of the tensile skeleton, as shown in Figure 6. $f_t$ is the peak tensile stress; $\varepsilon_{cr}$ is the strain corresponding to the peak tensile stress; $E_{c0}$ is the initial tangent modulus; and $\varepsilon_{ut}$ is the ultimate tensile strain.

The tensile damage index is calculated as follows [25]:

$$D_t = \begin{cases} 0, & \varepsilon_{cm}^{t} < \varepsilon_{cr}, \\ \dfrac{E_{c0} - E_{tm}}{E_{c0}}, & \varepsilon_{cr} \le \varepsilon_{cm}^{t} \le \varepsilon_{ut}, \\ 1, & \varepsilon_{ut} < \varepsilon_{cm}^{t}, \end{cases} \tag{2}$$

where $E_{tm}$ is the secant modulus of the current unloading point; $\varepsilon_{cm}^{t}$ is the strain at the current unloading point.

Tensile concrete damage only occurs during loading and does not occur during unloading. New damage occurs only after reloading reaches the previous unloading point. The stress-strain relationship and corresponding tensile damage index of concrete under tension are shown in Figure 7.

The parameters of the concrete material are shown in Table 4.

*3.2.2. Constitutive Model for Steel Material.* In the analysis of this study, the stress-strain relationship of steel bars was expressed by the modified Menegotto-Pinto constitutive model [33]. The model was proposed by Menegotto and Pinto and modified by Filippou et al. [34] to consider the influence of the isotropic strengthening effect. The Bauschinger effect under cyclic loads is considered in the model,

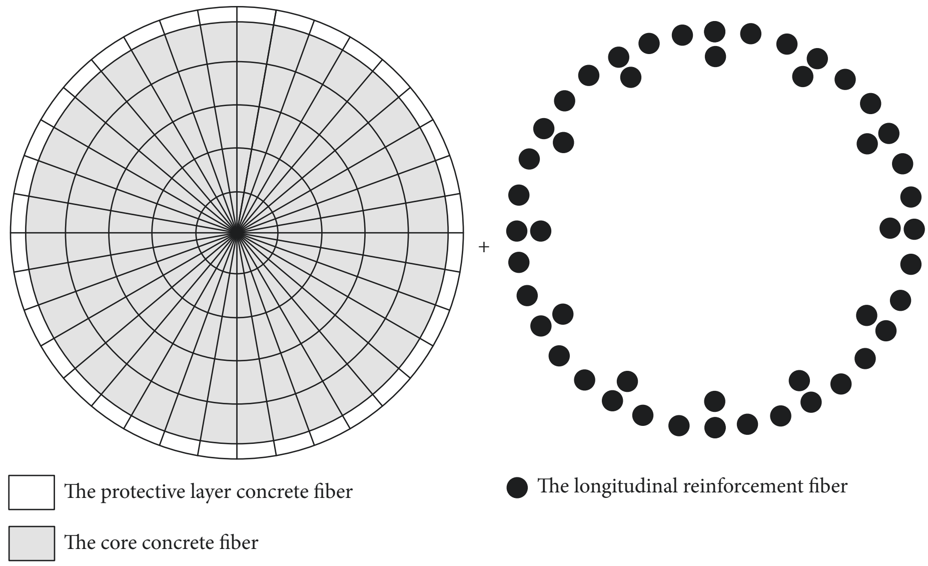


Figure 3: The cross-sectional fiber discretization method.

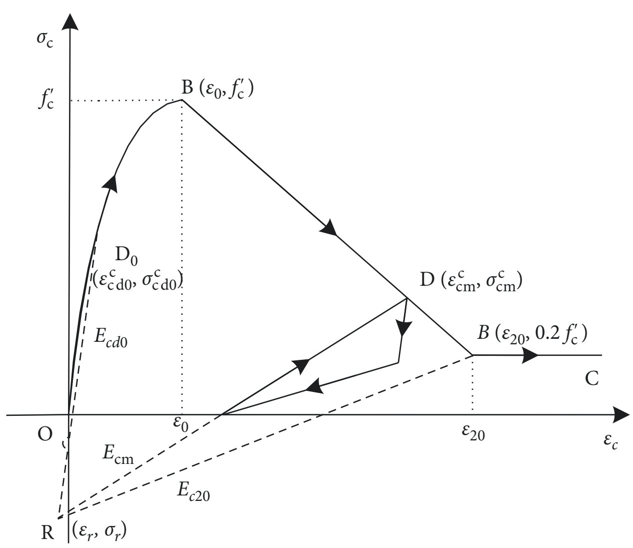


Figure 4: Yassin's concrete constitutive model.

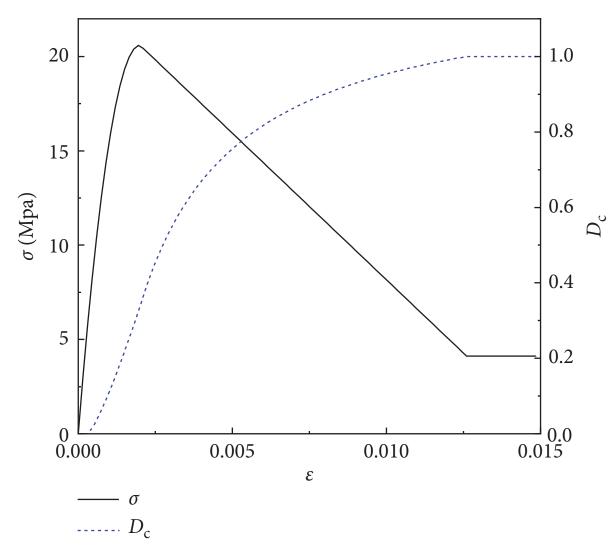


Figure 5: The compression damage index of concrete.

is in good agreement with experimental results, and has high solution efficiency. Overall, this model has been extensively used.

The Bonora damage model [35] was introduced into the modified Menegotto-Pinto constitutive model to consider the damage and fracture behavior of steel bars. The Bonora damage model is an elastic-plastic damage constitutive model based on continuous damage mechanics. The model adopts nonlinear damage evolution criteria, which can better simulate the damage performance of steel. Compared with the test, the model has high simulation accuracy. The damage index in the Bonora damage model is calculated as follows [35]:

$$\dot{D} = \alpha \frac{(D_{cr} - D_0)^{1/\alpha}}{\ln \varepsilon_{cr} - \ln \varepsilon_{th}} f\left(\frac{\sigma_m}{\sigma_{eq}}\right) (D_{cr} - D)^{\alpha - 1/\alpha} \frac{dp}{p}, \quad (3)$$

where $\dot{D}$ is the damage increment; $D$ is the cumulative damage value; $D_0$ is the initial damage value; $D_{cr}$ is the critical damage value; $\varepsilon_{cr}$ is the critical strain corresponding to the critical damage value; $\varepsilon_{th}$ is the threshold strain for the start of damage; $dp$ is equivalent plastic strain increment; $p$ is equivalent plastic strain; $\alpha$ is the damage parameter; and $f(\sigma_m/\sigma_{eq})$ is the influence factor in the triaxial stress state and is taken as 1 for the uniaxial constitutive model. The parameters used in this study are selected according to reference [35].

To account for the occurrence of repeated tension-compression overloads causing failure, Pirondi and Bonora [36] modified the Bonora damage model. It is considered that the steel bar is damaged only when it is tensile, so only the effect of tensile plastic strain is considered when calculating the damage index. Figures 8 and 9 are the stress-

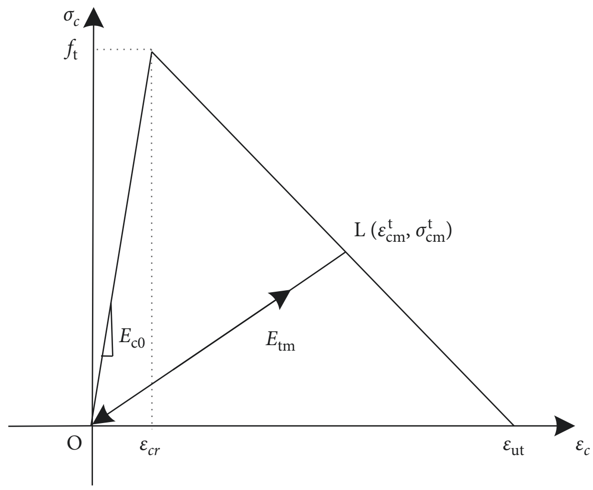


FIGURE 6: Tensile model of concrete.

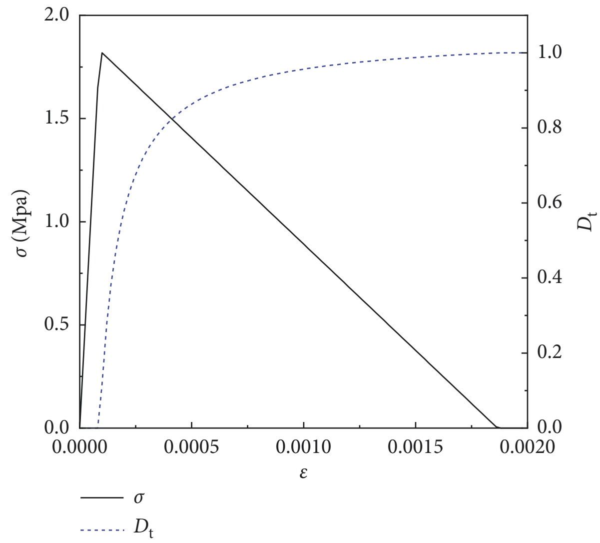


FIGURE 7: The tensile damage index of concrete.

strain relationship and corresponding damage index of steel under cyclic loading.

The parameters of the steel material are shown in Table 5.

TABLE 4: Parameters of the concrete material.

| Concrete | $f_c'$ (MPa) | $\varepsilon_0$ | $\varepsilon_{20}$ | $f_t$ (MPa) |
|---|---|---|---|---|
| Protective layer | −34.5 | −0.0025 | −0.006 | 3.65 |
| Core | −35.8 | −0.0028 | −0.0072 | 3.65 |

*3.2.3. Force-Displacement Response of a Pier.* The force-displacement response of a pier under a constant axial force of 2889.24 kN is shown in Figure 10. The horizontal bearing capacity of the pier is 1241.8 kN.

*3.3. Bearing Analysis Model.* Li et al. [17] developed an LRB isolation element model based on ABAQUS, which adopted the bidirectional coupled Bouc-Wen model improved by Casciati [37] in the horizontal direction. The restoring force was combined with the following relationship:

$$\begin{bmatrix} F_1 \\ F_2 \end{bmatrix} = \alpha k_b \begin{bmatrix} U_1 \\ U_2 \end{bmatrix} + (1-\alpha) F_y \begin{bmatrix} Z_1 \\ Z_2 \end{bmatrix} + c_b \begin{bmatrix} \dot{U}_1 \\ \dot{U}_2 \end{bmatrix}, \qquad (4)$$

where $F_1$ and $F_2$ are the restoring forces of the lead rubber bearings in the $X$ and the $Y$ directions, respectively; $U_1$ and $U_2$ represent the relative displacement of the lead rubber bearing in the $X$ and the $Y$ directions, respectively; $\alpha$ is the ratio of postyield-to-preyield stiffness; $k_b$ is the initial stiffness; $c_b$ is viscous damping of the lead rubber bearings; and $Z_1$ and $Z_2$ are the hysteretic displacements in the $X$ and the $Y$ directions, respectively, satisfying the following relationship:

$$U_y \begin{bmatrix} \dot{Z}_1 \\ \dot{Z}_2 \end{bmatrix} = [G] \begin{bmatrix} \dot{U}_1 \\ \dot{U}_2 \end{bmatrix}, \qquad (5a)$$

$$G = \begin{bmatrix} A - \beta \mathrm{sgn}\left(\dot{U}_1 Z_1 + \dot{U}_2 Z_2\right) Z_1^2 - \gamma Z_1^2 & -\beta \mathrm{sgn}\left(\dot{U}_1 Z_1 + \dot{U}_2 Z_2\right) Z_1 Z_2 - \gamma Z_1 Z_2 \\ -\beta \mathrm{sgn}\left(\dot{U}_1 Z_1 + \dot{U}_2 Z_2\right) Z_1 Z_2 - \gamma Z_1 Z_2 A & -\beta \mathrm{sgn}\left(\dot{U}_1 Z_1 + \dot{U}_2 Z_2\right) Z_2^2 - \gamma Z_2^2 \end{bmatrix}, \qquad (5b)$$

where $U_y$ is the yield displacement of the lead rubber bearing; $A$, $\gamma$, and $\beta$ are the parameters that control the shape and size of the restoring force-displacement hysteresis loop of the lead rubber bearing, generally taking 1, 0.5, and 0.5, respectively; and sgn is a symbolic function.

The overlap area method [38] was used to determine the bearing capacity (critical load) of the bearing under a given lateral displacement as follows:

$$P_{cr}' = \frac{A_r}{A_b} P_{cr}, \qquad (6)$$

where $P_{cr}'$ is the bearing capacity (critical load) of a lead rubber bearing considering the influence of lateral displacement; $A_r$ is the area of the overlapping part of the upper and lower sections of the bearing; $A_b$ is the cross-sectional area of the lead rubber bearing; and $P_{cr}$ is the bearing

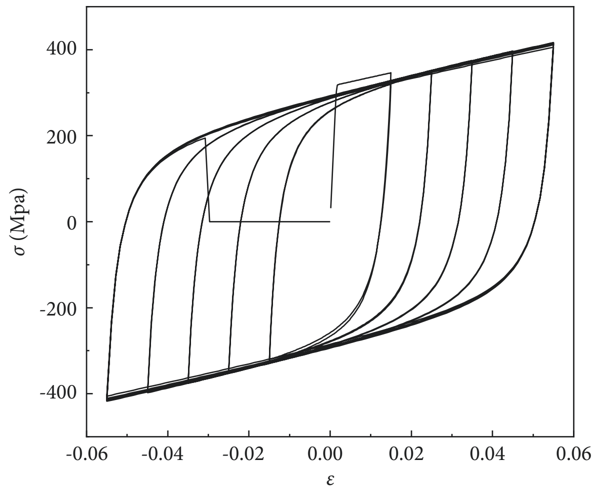


FIGURE 8: The stress-strain relationship of the steel.

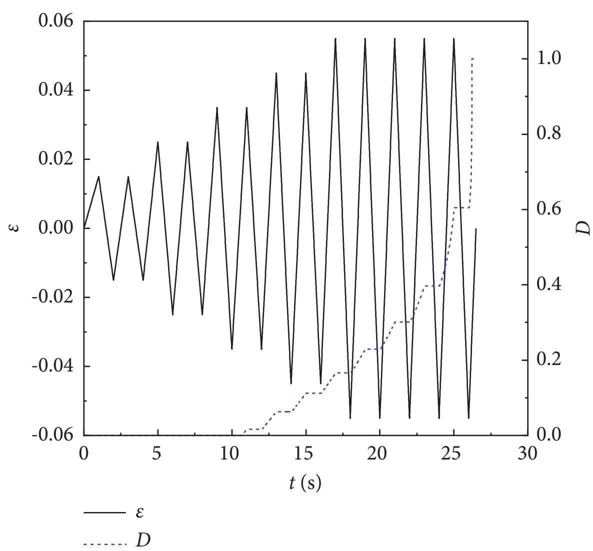


FIGURE 9: The damage index of the steel.

TABLE 5: Parameters of the steel material.

| $E_s$ (GPa) | $f_y$ (MPa) | $b$ | $\varepsilon_{th}$ | $\varepsilon_{cr}$ | $D_{cr}$ | $D_0$ | $\alpha$ |
|---|---|---|---|---|---|---|---|
| 210 | 303 | 0.01 | 0.259 | 1.4 | 0.065 | 0.0 | 0.2175 |

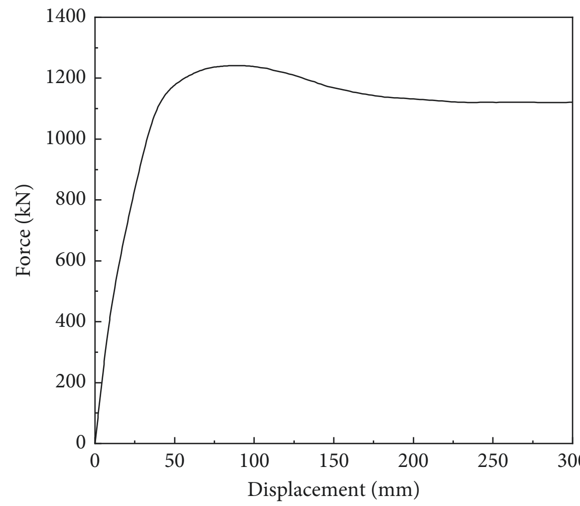


FIGURE 10: Force-displacement response of a pier.

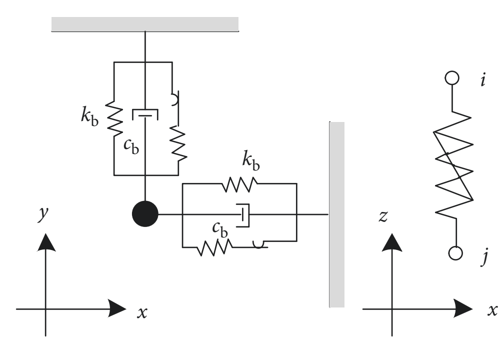


FIGURE 11: LRB isolation element model.

capacity (critical load) of the lead rubber bearing without lateral displacement.

The LRB isolation element model is shown in Figure 11.

## 4. Seismic Response Analysis of Bridges

Seismic responses of isolated and nonisolated bridges were analyzed, respectively, and the seismic responses of bridge structures under three different ground motions were studied. The spatial differential effect of ground motion was not considered in the analysis, and uniform excitation was used for ground motion input. The PGA in the *X* direction (*X* direction (longitudinal direction) of the bridge) of the selected ground motion record was uniformly adjusted to 0.4 g to correspond to a rare earthquake of 8 degrees [39]. The PGA in the *Y* direction (*Z* direction (transversal direction) of the bridge) was uniformly adjusted to 0.34 g. The PGA in the *Z* direction (*Y* direction (vertical direction) of the bridge) was uniformly adjusted to 0.26 g.

*4.1. Girder Acceleration.* Figures 12–14, respectively, show the peak acceleration responses of the girders at the top of the bearings of nonisolated bridges and isolated bridges under different types of ground motions. Overall, the peak accelerations at all positions of nonisolated bridges and isolated bridges were the same under the same ground motion in the *X* direction, regardless of the fling-step ground motions, forward-directivity ground motions, or far-field ground motions. Under the same ground motion in the *Y* direction, the peak acceleration at each position of the nonisolated bridge had a *W*-shaped distribution, while the peak acceleration at each position of the isolated bridge was the same. Under the different ground motions, the peak acceleration response of the bridges in the *Z* direction was greater than that in the *X* direction in most conditions, although the peak acceleration in the *X* direction was more significant when ground motions were input. This was more obvious at the end of nonisolated bridges. The *X*-direction acceleration of the B02 position of the nonisolated bridge

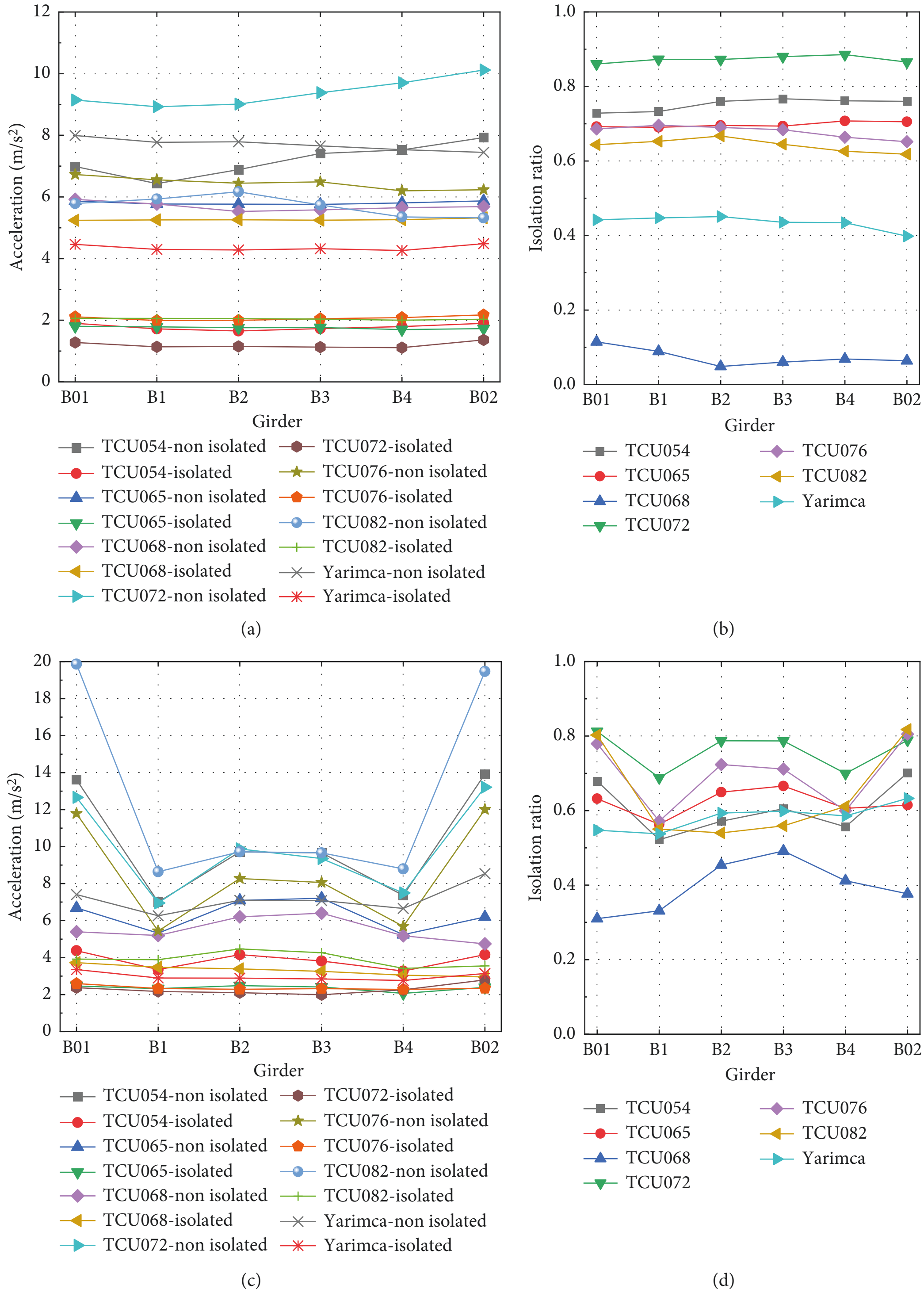


Figure 12: Peak acceleration of the girders under fling-step ground motions. (a) Peak acceleration in the $X$ direction. (b) Isolation ratio in the $X$ direction. (c) Peak acceleration in the $Z$ direction. (d) Isolation ratio in the $Z$ direction.

under the fling-step ground motion TCU072 reached $10.12\,m/s^2$, which is 2.53 times larger than the input $4.00\,m/s^2$. The $Z$-direction acceleration of the B01 position of the nonisolated bridge under the fling-step ground motion TCU082 reached $19.87\,m/s^2$, which is 5.84 times larger than the input of $3.40\,m/s^2$.

For the fling-step ground motions, under TCU068 ground motion, the isolation effect of the isolation bearings was the least in the $X$ direction and $Z$ direction, especially in the $X$ direction, with the lowest isolation ratio being only 0.06. This indicates that the isolation bearings hardly affected the structure concerning seismic isolation. Except under the

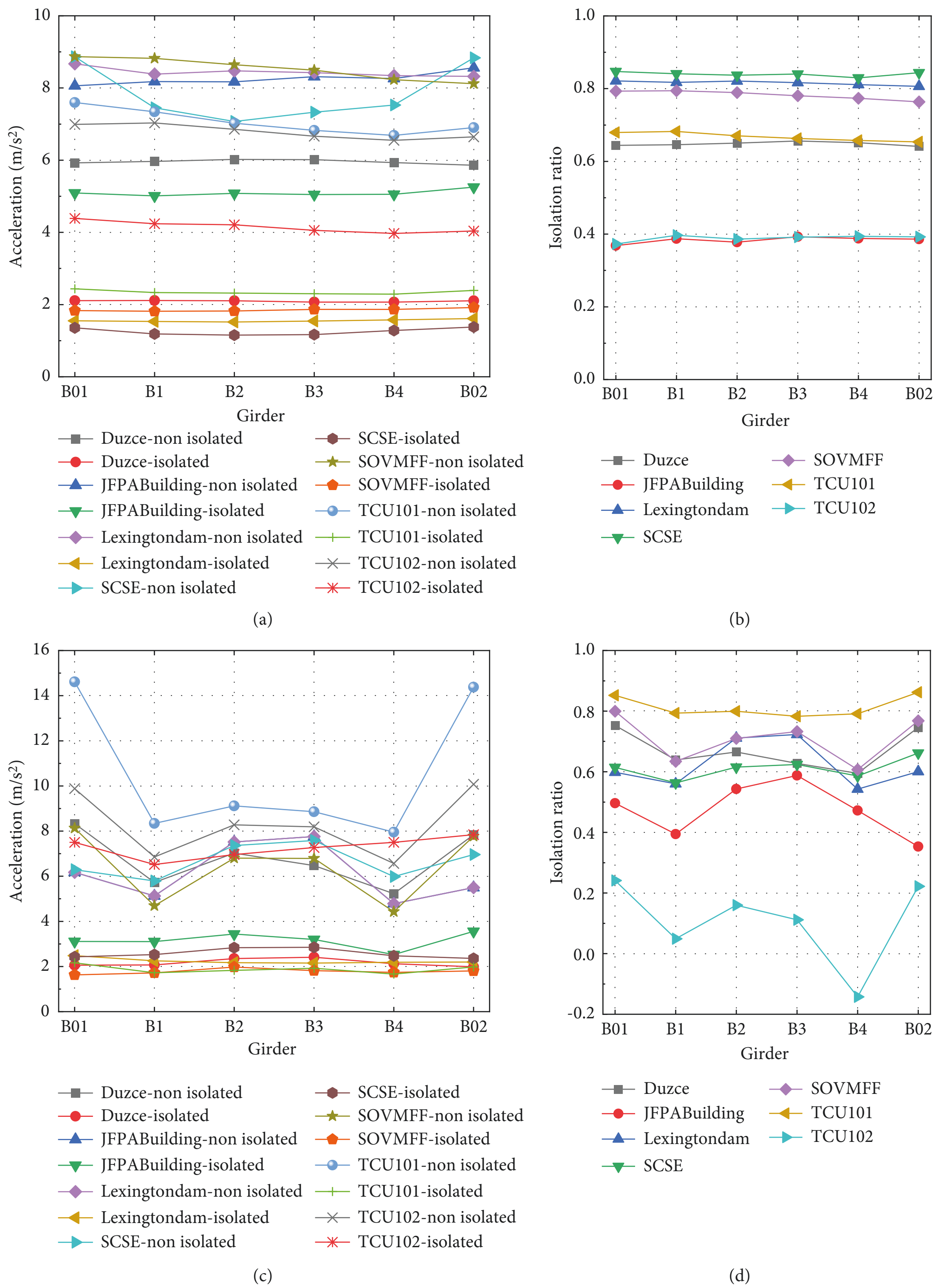


Figure 13: Peak acceleration of the girders under forward-directivity ground motions. (a) Peak acceleration in the $X$ direction. (b) Isolation ratio in the $X$ direction. (c) Peak acceleration in the $Z$ direction. (d) Isolation ratio in the $Z$ direction.

Yarimca ground motion, the isolation ratios of the isolation bearings in the $X$ direction were slightly lower, ranging from 0.4 to 0.5. The isolation effect of the isolation bearings under other ground motions increased, with all ratios greater than 0.5. Under the TCU072 ground motion, the isolation effect of the isolation bearings was the greatest, with a maximum isolation ratio reaching 0.89.

For the forward-directivity ground motions, under JFPABuilding and TCU102 ground motion, the isolation effects of the isolation bearings in the $X$ direction were

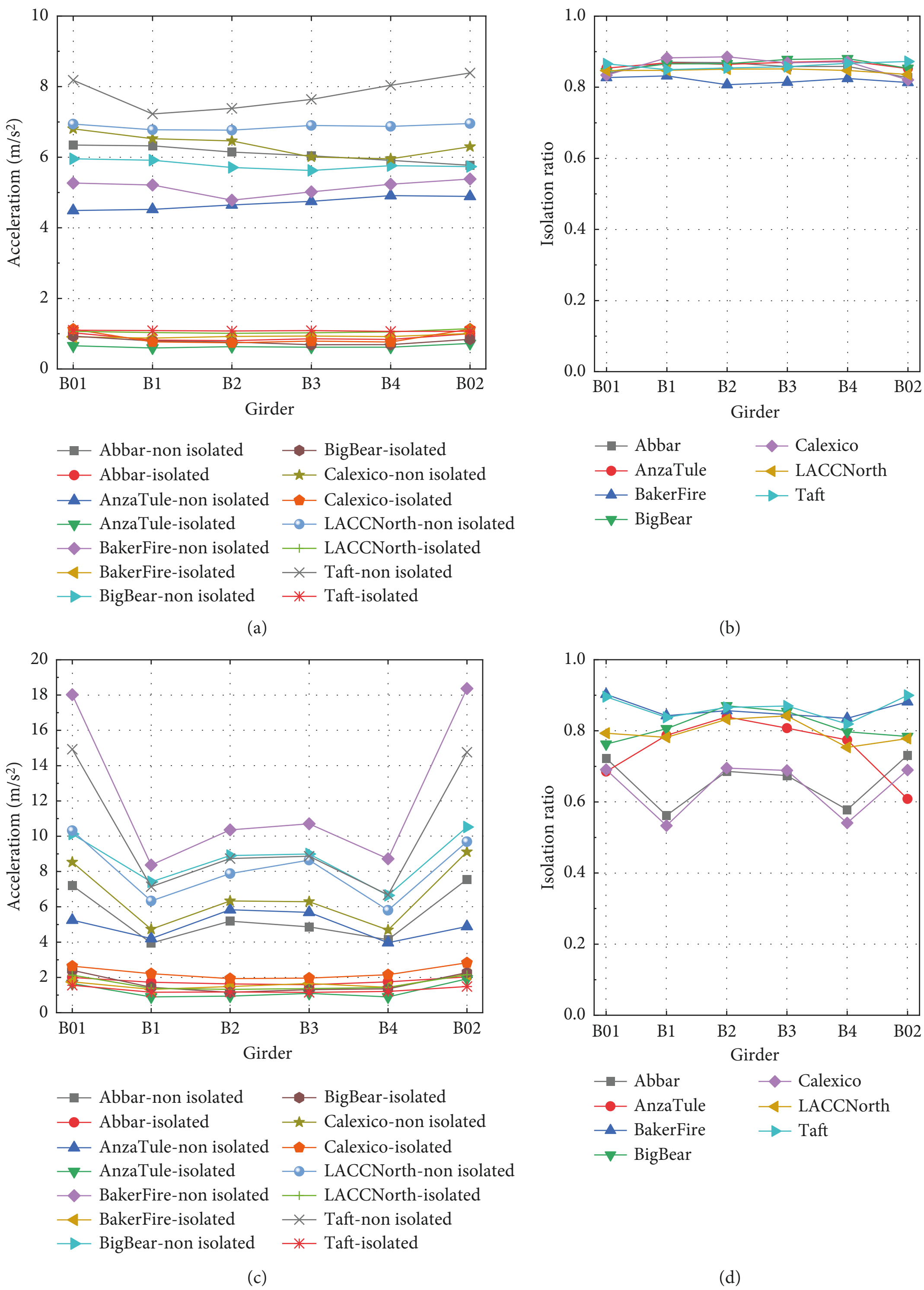


FIGURE 14: Peak acceleration of the girders under far-field ground motions. (a) Peak acceleration in the $X$ direction. (b) Isolation ratio in the $X$ direction. (c) Peak acceleration in the $Z$ direction. (d) Isolation ratio in the $Z$ direction.

relatively poor, with isolation ratios of ~0.4. Under other ground motions, the isolation effects of the isolation bearings increased, with the isolation ratios all greater than 0.6. The isolation ratios of the isolation bearings were greater than 0.6 under only three ground motions in the $Z$ direction. Under the TCU102 ground motion, the isolation effect of the isolation bearings was the least. Even at the B4 position, the isolation ratio was −0.14, indicating that the isolation bearing did not reduce the acceleration response; instead, it increased the acceleration response. This shows that the isolation bearings cannot be used under TCU102 ground motion.

Under the far-field ground motions, the isolation effects of the isolation bearings were excellent in the $X$ direction. The isolation ratios were all above 0.8; the isolation bearings had a good isolation effect in the $Z$ direction, and the lowest isolation ratio was still greater than 0.5.

*4.2. Pier Displacement.* Figures 15–17 show the peak displacement of piers of nonisolated bridges and isolated bridges under different types of ground motions, respectively. The displacement of the pier was calculated by $\sqrt{D_X^2 + D_Z^2}$ (where $D_X$ and $D_Z$ are the displacements of the pier in the $X$ and $Z$ directions, respectively). The peak displacements of the middle piers of the nonisolated bridges were slightly greater than that of the side piers under the same ground motion, regardless of the fling-step ground motions, forward-directivity ground motions, or far-field motions. However, the peak displacements of the isolated bridge piers were the same. Under the fling-step ground motions, the maximum peak displacement and the minimum peak displacement of nonisolated bridge piers were 219.49 mm and 95.86 mm, respectively. The maximum peak displacement of isolated bridge piers was 98.40 mm, and the minimum peak displacement was 7.42 mm. Under the forward-directivity ground motions, the maximum peak displacement of nonisolated bridge piers was 271.67 mm, and the minimum peak displacement was 77.95 mm. The maximum peak displacement of the isolated bridge piers was 715.49 mm, and the minimum peak displacement was 9.91 mm. Under the far-field ground motions, the maximum peak displacement of nonisolated bridge piers was 169.75 mm, and the minimum peak displacement was 39.07 mm. The maximum peak displacement of the isolated bridge piers was 8.75 mm, and the minimum peak displacement was 2.65 mm. The maximum peak displacement and minimum peak displacement of the nonisolated bridge piers under fling-step ground motion and forward-directivity ground motion were more extensive than those under far-field ground motion. The maximum peak displacement of the isolated bridge piers under fling-step ground motion and the forward-directivity ground motion was much larger than that under far-field ground motion, especially under forward-directivity ground motion. The minimum peak displacement of the isolated bridge piers under fling-step ground motion and the forward-directivity ground motion was much larger than that under far-field ground motions, but its values were overall small.

For the fling-step ground motions, under TCU068 ground motion, the isolation effect of the isolation bearings was very poor, with the lowest isolation ratio of only 0.13. This indicates that the isolation bearings have little influence on seismic isolation. Under other ground motions, the isolation effects of the isolation bearings were better, with ratios all above 0.7 and a maximum of 0.96. For the forward-directivity ground motions, except under TCU102 ground motion, the isolation effects of isolation bearings under other ground motions were better, with the isolation ratios all greater than 0.7. The isolation bearings do not affect seismic isolation under TCU102 ground motion. The isolation ratio of each position was negative, below −1.86, with a minimum of −2.65. This shows that the isolation bearings do not reduce the displacement response of piers but significantly increase the displacement response of piers. The isolation bearings cannot be used under TCU102 ground motion. Under the far-field ground motions, the isolation effects of isolation bearings were outstanding, and the isolation ratios were all above 0.9.

*4.3. Pier Shear Force.* Figures 18–20 show the peak shear force of piers of nonisolated bridges and isolated bridges under different ground motions. The peak shear force of each pier of the nonisolated bridge reached the maximum bearing capacity of the pier of ~ 1200 kN under the fling-step ground motions, forward-directivity ground motions, or far-field ground motions. The difference in the maximum bearing capacity of piers is caused by a difference in the vertical loads on the piers. For the fling-step ground motions, under the TCU072 ground motion, the isolation bearings significantly reduce the peak shear force of the piers, with a minimum value of 352.25 kN. Under the TCU068 ground motion, the isolation bearings did not reduce the peak shear force of the piers, with the peak shear force of the piers above 1200 kN. For the forward-directivity ground motions, except under JFPABuilding and TCU102 ground motions, the isolation bearings significantly reduced the peak shear force of the piers under other ground motions, and their values were between 400 kN and 600 kN. Under JFPABuilding and TCU102 ground motions, the isolation bearings did not reduce the peak shear force of each pier, with the peak shear force of each pier ~1200 kN. Under the far-field ground motions, the isolation bearings significantly reduced the peak shear force of piers, and the peak shear force of each pier was below 400 kN.

The isolation effect of the isolation bearing under TCU068 fling-step ground motion was minor, with the lowest isolation ratio being −0.01. This indicates that the isolation bearings do not play roles in seismic isolation. The isolation bearings under the TCU068 ground motion were not applicable. The isolation effect of the isolation bearing under the Yarimca ground motion was also poor, with the isolation ratios all less than 0.2. The isolation effects of the isolation bearings under other ground motions increased with ratios ranging between 0.4 and 0.75. For the forward-directivity ground motion, the isolation effect of the isolation bearing under TCU102 ground motion was poor, with the lowest isolation ratio being −0.05. This indicates that the isolation bearings do not contribute to seismic isolation. The isolation bearing under TCU102 ground motion was not applicable. The isolation effect of the bearings under the JFPABuilding ground motion was poor, with the isolation ratios all less than 0.1. The isolation effects of the isolation bearings under other ground motions were improved, with isolation ratios between 0.5 and 0.7. Under the far-field ground motions, the isolation effects of the isolation bearings were excellent, with isolation ratios all above 0.7.

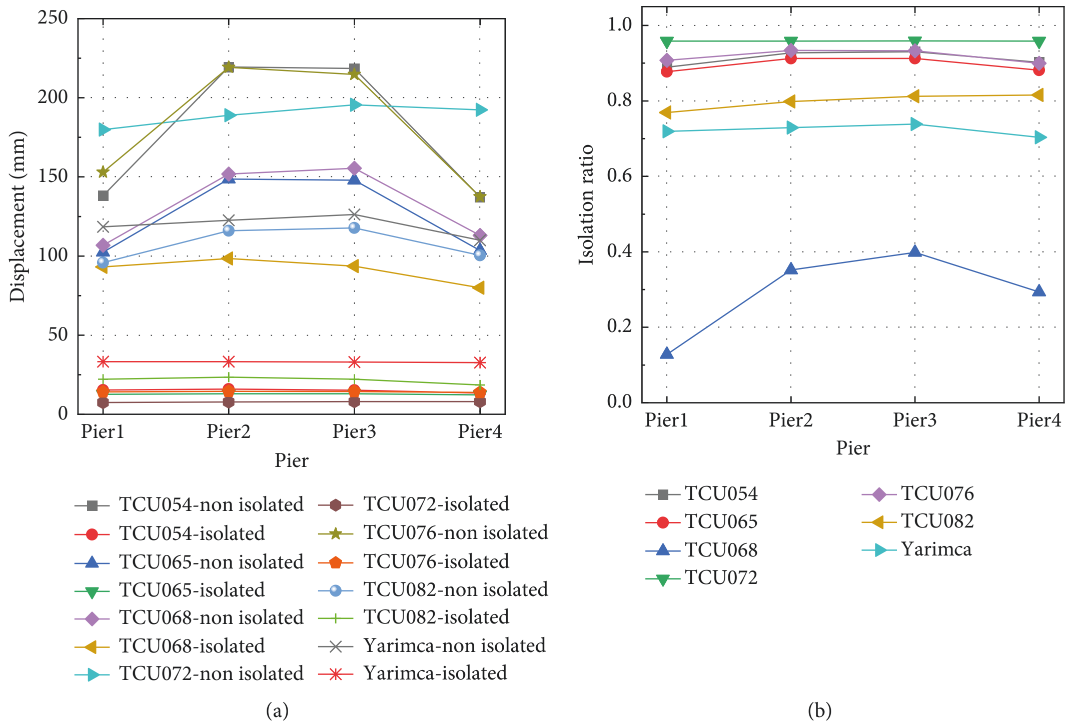


FIGURE 15: Peak displacement of piers under fling-step ground motions. (a) Peak displacement. (b) Isolation ratio.

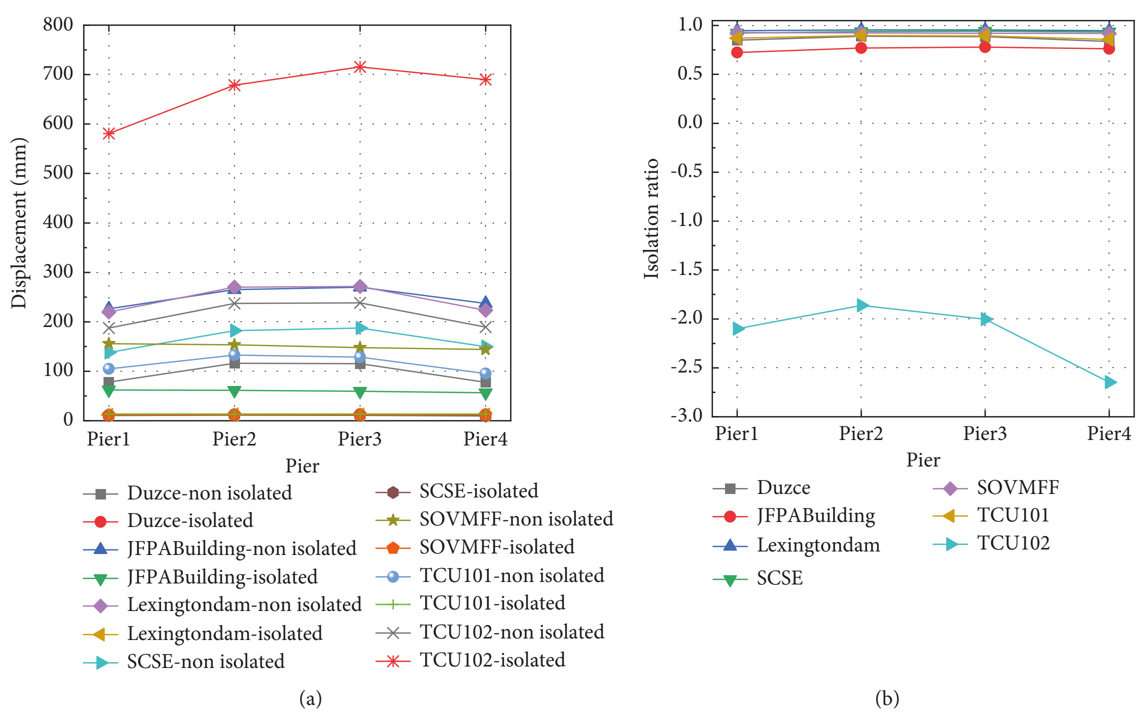


FIGURE 16: Peak displacement of piers under forward-directivity ground motions. (a) Peak displacement. (b) Isolation ratio.

*4.4. Pier Damage.* Under various conditions, the reinforcement damage of each pier was either negligible or nonexistent. The tensile damage index of concrete quickly reached 1; therefore, only the compression damage of concrete in the core area was analyzed. Based on the method Heo and Kunnath [20] proposed for estimating the damage index of the concrete member, the damage index of the pier was estimated using the damage index of the most critical fibers for concrete in the core area and reinforcing steel. Because the reinforcement damage of each pier was very

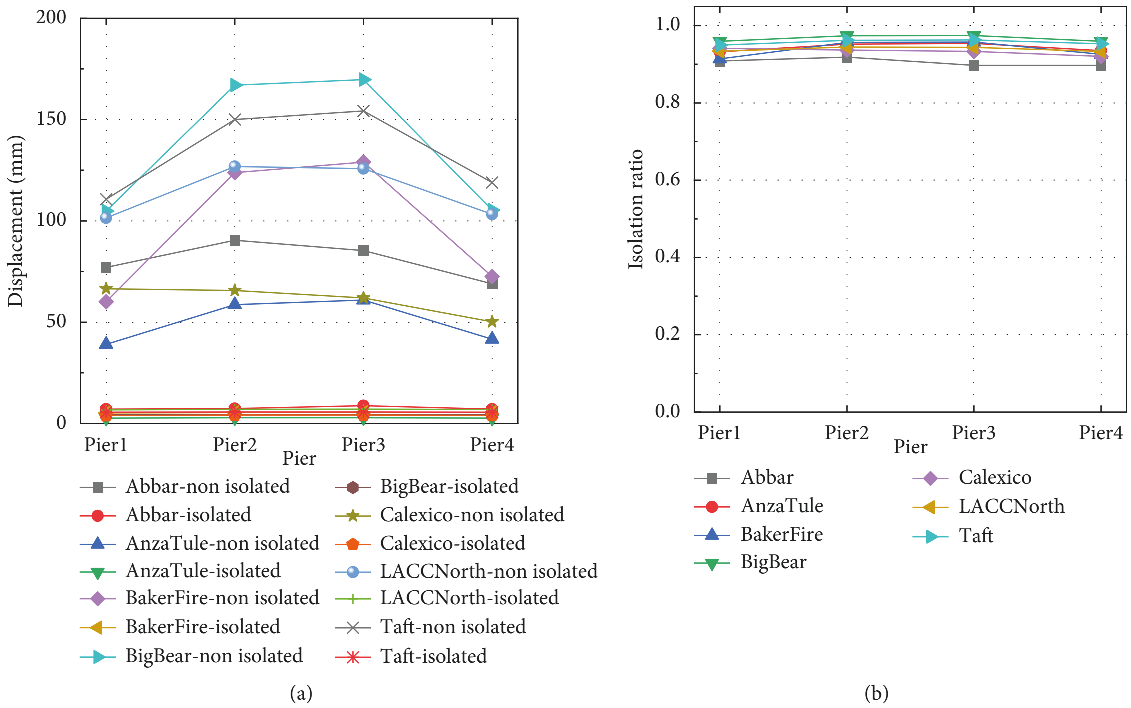


FIGURE 17: Peak displacement of piers under far-field ground motions. (a) Peak displacement. (b) Isolation ratio.

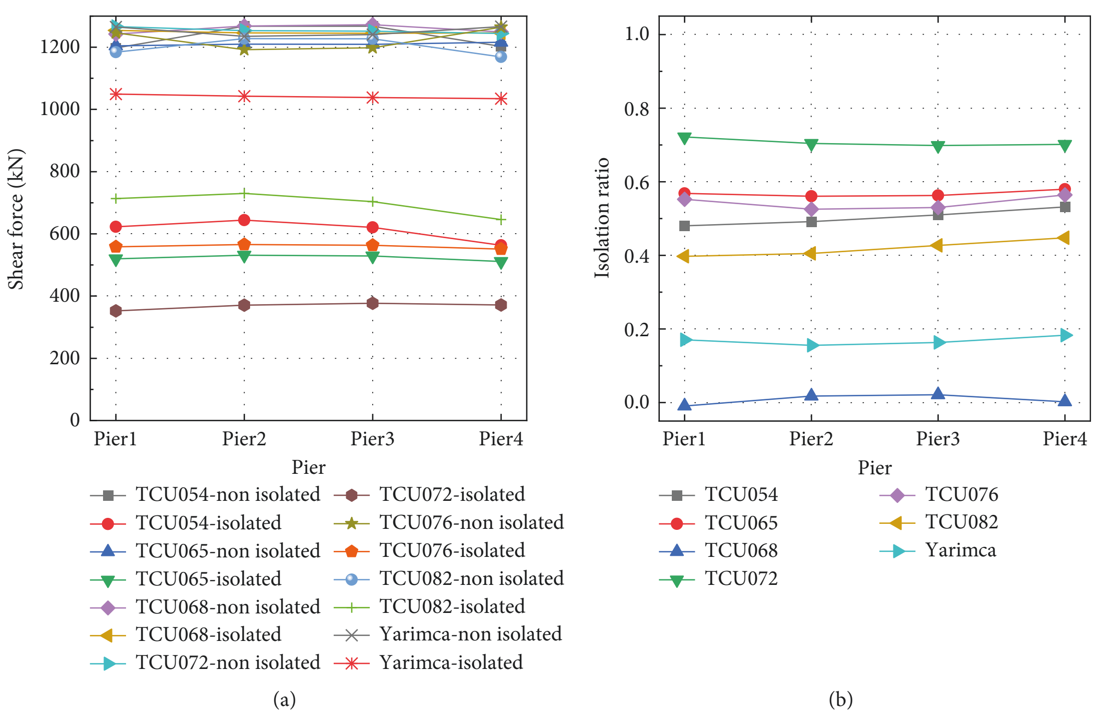


FIGURE 18: Peak shear force of piers under fling-step ground motions. (a) Peak shear force. (b) Isolation ratio.

small or none, it was reasonable to consider the damage index of the most critical fiber for concrete in the core area as the representative damage index of the pier.

Figures 21–23, respectively, show the peak damage index of the compression concrete in the pier core area of nonisolated bridges and isolated bridges under different ground motions. Under the same ground motion, the peak damage indexes of the middle piers were slightly greater than that of the side piers for the nonisolated bridge, regardless of the fling-step ground motions, forward-directivity ground

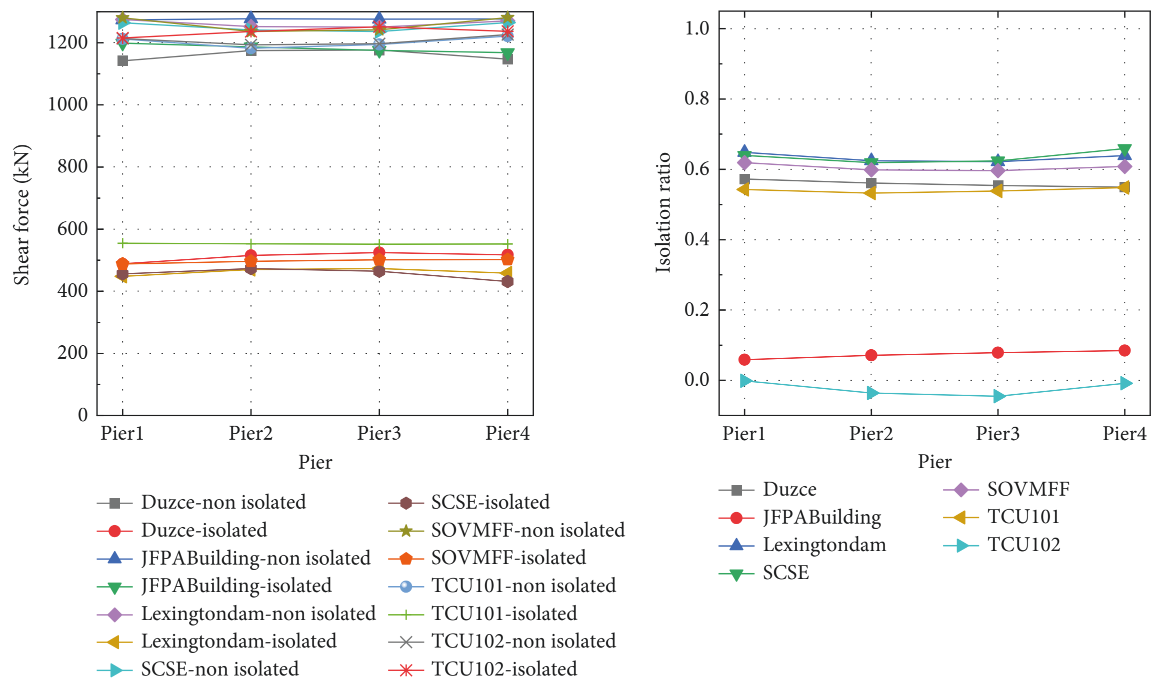


(a) (b)

FIGURE 19: Peak shear force of piers under forward-directivity ground motions. (a) Peak shear force. (b) Isolation ratio.

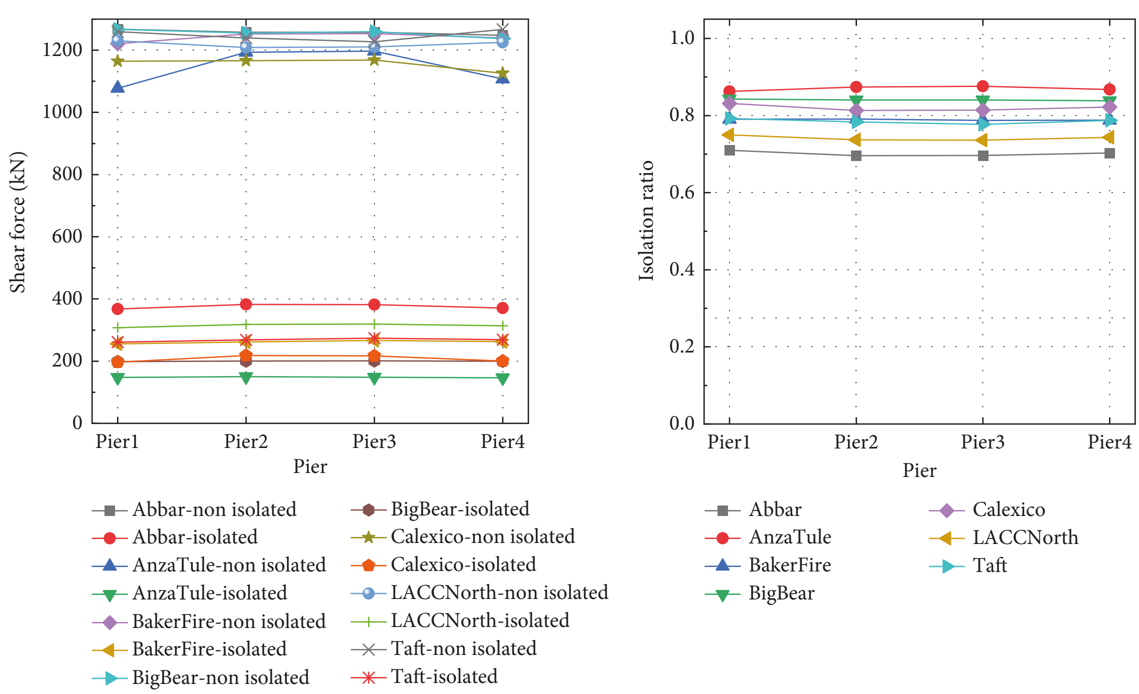


(a) (b)

FIGURE 20: Peak shear force of piers under far-field ground motions. (a) Peak shear force. (b) Isolation ratio.

motions, or far-field motions. However, the peak damage index to each pier of the isolated bridge was the same. This is consistent with the peak displacement response of piers.

Under the TCU072 and TCU076 fling-step ground motions, the peak damage index of each pier of the nonisolated bridge reached 1; the concrete in the core area of each pier was crushed. Under TCU054, TCU065, and TCU068 ground motions, the peak damage index of the middle piers (P2 and P3) of the nonisolated bridge also reached 1, indicating that the area was also destroyed. Under

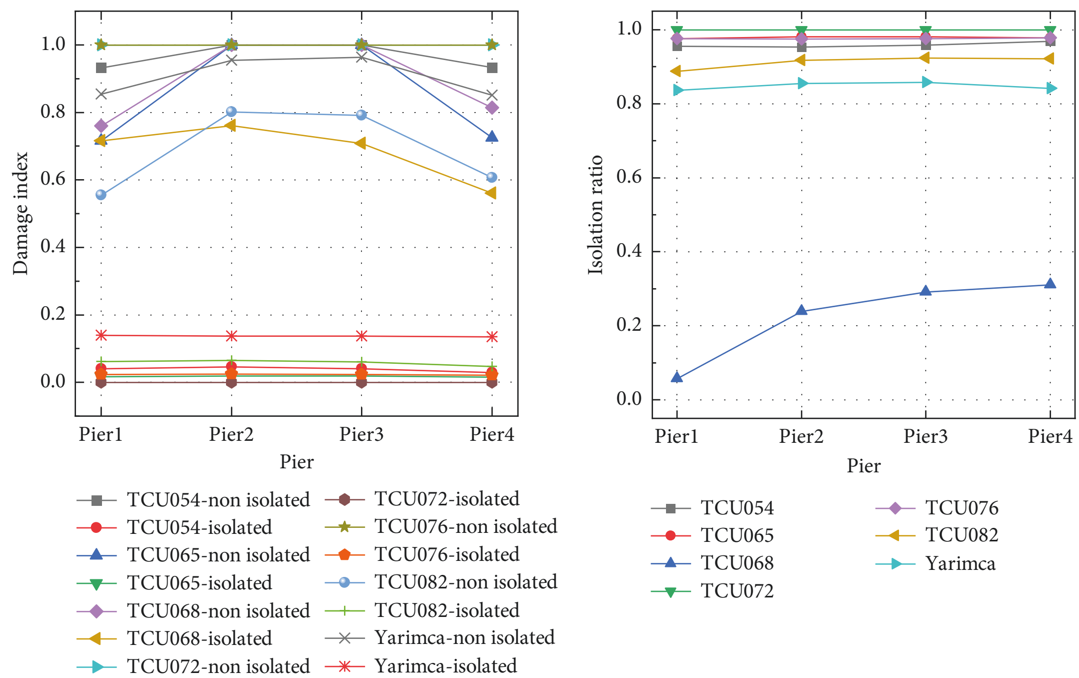


(a) (b)

FIGURE 21: Peak damage index of concrete in the pier core area under fling-step ground motions. (a) Peak damage index. (b) Isolation ratio.

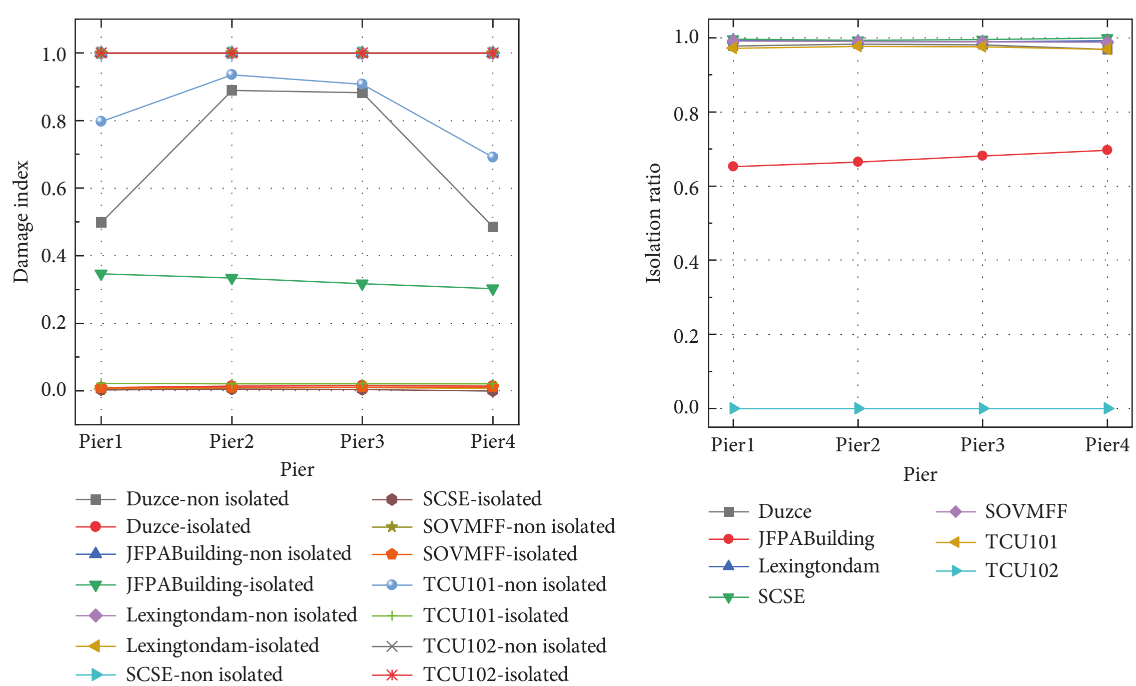


(a) (b)

FIGURE 22: Peak damage index of concrete in the pier core area under forward-directivity ground motions. (a) Peak damage index. (b) Isolation ratio.

the Yarimca ground motion, the peak damage index of each pier of the nonisolated bridge did not reach 1 but was greater than 0.85, indicating extensive damage to the pier. Under the TCU082 ground motion, the peak damage index of each pier of the nonisolated bridge was relatively small, ranging from 0.5 to 0.8. Under the TCU068 ground motion, the peak damage indexes of the isolated bridge ranged between 0.5 and 0.8, indicating extensive damage. Under other ground

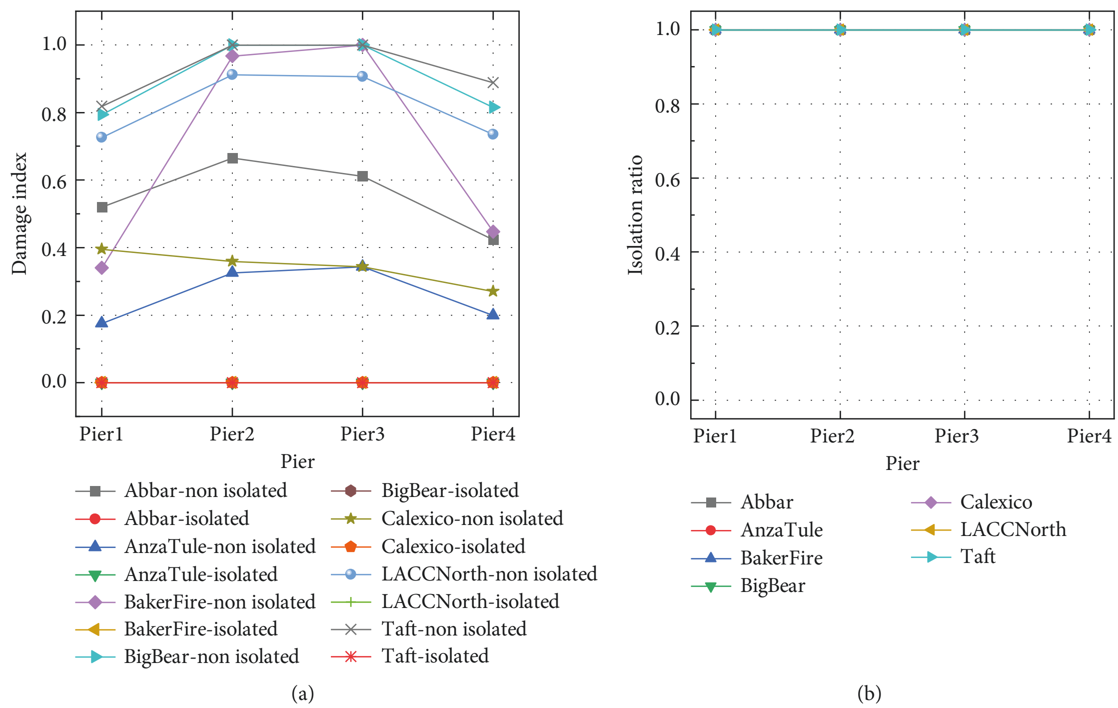


Figure 23: Peak damage index of concrete in the pier core area under far-field ground motions. (a) Peak damage index. (b) Isolation ratio.

motions, the peak damage index of each pier of the isolated bridge was less than 0.15, indicating very little damage to the piers.

For the forward-directivity ground motions, although the peak damage indexes of the piers (P2 and P3) of the nonisolated bridge under Duzce and TCU101 ground motions did not reach 1, they were greater than 0.85, showing significant damage to the piers. The peak damage indexes of the side piers (P1 and P4) were relatively small, but they still varied between 0.45 and 0.8. Under other ground motions, the peak damage index of each pier of the nonisolated bridge reached 1, indicating complete destruction to the core. Under the TCU102 ground motion, the peak damage index of each isolated bridge pier reached 1, indicating that the concrete in the core area of each pier was crushed, and the isolation bearings do not play a role in reducing the damage to the pier. Under the JFPABuilding ground motion, the peak damage index of each isolated bridge pier varied between 0.3 and 0.35, and the damage to each pier was relatively minor. Under other ground motions, the peak damage index of each isolated bridge pier was less than 0.03, and the damage to each pier was minimal.

Under the BigBear and Taft far-field ground motions, the peak damage indexes of the middle piers (P2 and P3) of the nonisolated bridge reached 1, and the concrete core area was crushed. Although the peak damage indexes of the side piers (P1 and P4) did not reach 1, there were still above 0.8, indicating extensive damage to the piers. Under the BakerFire ground motion, the peak damage index of pier P3 of the nonisolated bridge reached 1, and the concrete in the core area of the pier was crushed. The peak damage index of pier P2 reached 0.97. Although the concrete in the core area of pier P2 was not crushed, it was extensively damaged. The peak damage indexes of the side piers (P1 and P4) ranged between 0.3 and 0.45, and the damage was relatively small. Under the LaCCNth ground motion, the peak damage indexes of the middle piers (P2 and P3) of the nonisolated bridge were greater than 0.9, and the peak damage indexes of the side piers (P1 and P4) were above 0.7. Each pier has extensive damage. Under other ground motions, the peak damage index of each pier of the nonisolated bridge was less than 0.7, with a minimum value of 0.18; here, the pier damage is relatively minor. Under the far-field ground motions, the peak damage index of each pier of the isolated bridge was 0, and there was no compression damage to the concrete in the core area of each pier.

The lowest isolation ratio under the TCU068 fling-step ground motion was only 0.06. Here, the isolation effects of the isolation bearings were minimal, and the isolation bearings hardly affected the seismic isolation of the bridge. Under other ground motions, the isolation ratios were greater than 0.8, and the maximum even reached 1. The isolation bearings were effective under these ground motions. For the forward-directivity ground motions, the isolation ratio of each isolation bearing under the TCU102 ground motion was 0, and the isolation bearings did not influence seismic isolation. The isolation ratios under the JFPABuilding ground motion were between 0.65 and 0.7, and the isolation effects of the isolation bearings were moderate. The isolation ratios under other ground motions were greater than 0.95, and the isolation effects of isolation bearings were significant. Under far-field ground motions, all the isolation ratios reached 1, and isolation bearings were very effective.

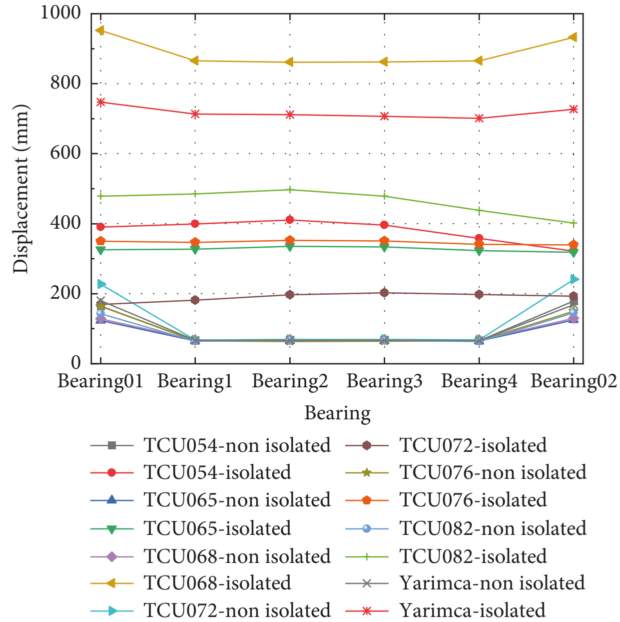


Figure 24: Peak displacement of bearings under fling-step ground motions.

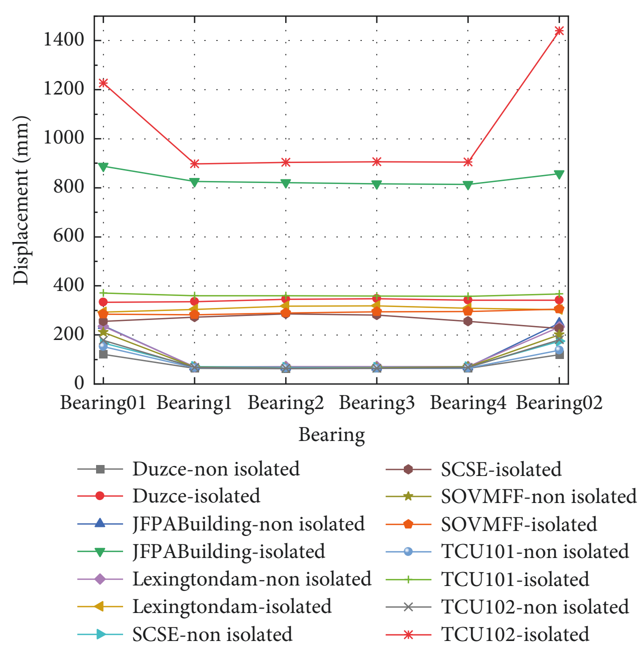


Figure 25: Peak displacement of bearings under forward-directivity ground motions.

### *4.5. Bearing Response*

*4.5.1. Bearing Displacement.* Figures 24–26 show the peak displacement of bearings of nonisolated bridges and isolated bridges under different types of ground motions. The peak displacement of the middle bearings (Bearing1~Bearing4) of the nonisolated bridge under various ground motions was ~65 mm. Under the fling-step ground motions, forward-directivity ground motions, and far-field ground motions, the maximum peak displacements of the end bearings (Bearing01 and Bearing02) were 240.95 mm, 249.04 mm, and 172.08 mm, respectively. The peak displacements of the end bearings of the nonisolated bridges were much larger than those of the middle bearings. The peak displacements of all bearings of the isolated bridges were the same under the same ground motion.

For the fling-step ground motions, the peak displacements of the end bearings (Bearing01 and Bearing02) of the isolated bridge under the TCU072 ground motion were slightly smaller than those of the nonisolated bridge. The peak displacements of the middle bearings (Bearing1~Bearing4) of the isolated bridge were much larger than

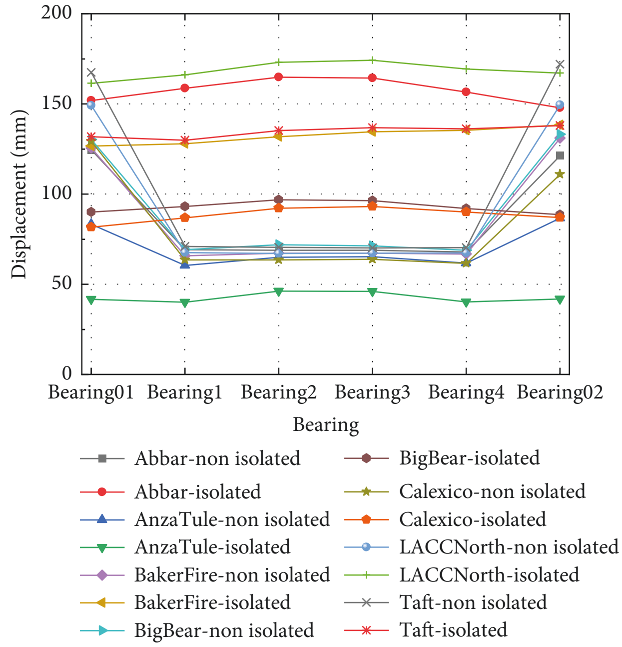


Figure 26: Peak displacement of bearings under far-field ground motions.

Table 6: Failure of isolation bearings under different types of ground motions.

| | | | Fling-step ground motions | | | | |
|---|---|---|---|---|---|---|---|
| Bearing | TCU054 | TCU065 | TCU068 | TCU072 | TCU076 | TCU082 | Yarimca |
| Bearing01 | 1 | 0 | 1 | 0 | 0 | 1 | 1 |
| Bearing1 | 1 | 1 | 1 | 0 | 1 | 1 | 1 |
| Bearing2 | 1 | 1 | 1 | 1 | 1 | 1 | 1 |
| Bearing3 | 1 | 1 | 1 | 1 | 1 | 1 | 1 |
| Bearing4 | 1 | 1 | 1 | 1 | 1 | 1 | 1 |
| Bearing02 | 0 | 0 | 1 | 0 | 0 | 1 | 1 |
| | | | Forward-directional ground motions | | | | |
| Bearing | Duzce | JFPABuilding | Lexington Dam | SCSE | SOVMFF | TCU101 | TCU102 |
| Bearing01 | 0 | 1 | 0 | 0 | 0 | 0 | 1 |
| Bearing1 | 1 | 1 | 1 | 1 | 1 | 1 | 1 |
| Bearing2 | 1 | 1 | 1 | 1 | 1 | 1 | 1 |
| Bearing3 | 1 | 1 | 1 | 1 | 1 | 1 | 1 |
| Bearing4 | 1 | 1 | 1 | 1 | 1 | 1 | 1 |
| Bearing02 | 0 | 1 | 0 | 0 | 0 | 0 | 1 |
| | | | Far-field ground motions | | | | |
| Bearing | Abbar | AnzaTule | BakerFire | BigBear | Calexico | LaCCNth | Taft |
| Bearing01 | 0 | 0 | 0 | 0 | 0 | 0 | 0 |
| Bearing1 | 0 | 0 | 0 | 0 | 0 | 0 | 0 |
| Bearing2 | 0 | 0 | 0 | 0 | 0 | 0 | 0 |
| Bearing3 | 0 | 0 | 0 | 0 | 0 | 0 | 0 |
| Bearing4 | 0 | 0 | 0 | 0 | 0 | 0 | 0 |
| Bearing02 | 0 | 0 | 0 | 0 | 0 | 0 | 0 |

those of the nonisolated bridge. Under other ground motions, the peak displacement of each bearing of the isolated bridge was much larger than that of the nonisolated bridge. Especially under the TCU068 and Yarimca ground motions, the maximum peak displacement of the bearings of the isolated bridges reached 952.45 mm and 747.39 mm, respectively. Under other ground motions, the peak displacement of the isolated bridge bearings ranged between 300 mm and 500 mm.

Under the forward-directivity ground motions, the peak displacement of each isolated bridge bearing was much larger than that of the nonisolated bridge. Especially under the TCU102 and JFPABuilding ground motions, the maximum peak displacement of the isolated bridge bearings reached 1441.05 mm and 888.34 mm, respectively. Under other ground motions, the peak displacement of the isolated bridge bearings ranged between 200 mm and 400 mm. For the far-field ground motions, the peak displacement of each isolated bridge bearing was smaller than that of the nonisolated bridge under the AnzaTule ground motion. Under the BigBear, Calexico, and Taft ground motions, the peak displacement of the end bearings of the isolated bridges (Bearing01 and Bearing02) was slightly less than that of nonisolated bridges. Under other ground motions, the peak displacement of the bearings of the isolated bridges was more significant than that of nonisolated bridges. However, the maximum peak displacement of the bearings of the isolated bridges was only 174.23 mm. This value was slightly larger than the minimum value of the bearing peak displacement of the isolated bridge under the fling-step ground motion, reaching 169.98 mm, and smaller than the minimum value of 227.18 mm for the bearing peak displacement of the isolated bridge under the forward-directivity ground motion.

*4.5.2. Failure of Isolation Bearings.* The failure of isolation bearings under different types of ground motions is given in Table 6. Here, 0 indicates that the isolation bearing was not damaged, and 1 indicates that the isolation bearing was damaged. The failure index of the bearing model was only used for identification in the analysis, and the mechanical properties of the bearing were not affected. Most of the isolation bearings were damaged under the ground motion of the fling step and forward directivity; only 8 and 10 isolation bearings were not damaged, respectively. All isolation bearings were not damaged under the far-field ground motions. Overall, this shows that an isolation bearing cannot be directly used under near-field conditions.

## 5. Discussion

This study found that the isolation bearings can effectively reduce various seismic responses of the bridge under the far-field ground motions. Under the near-field ground motions, the isolation bearings still have a specific isolation effect in most cases, consistent with Jonsson et al.'s [6] and Wei et al.'s [7] research results. At the same time, it was found that the isolation bearings do not work and even amplified the seismic response of the bridge, such as under the fling-step TCU068 ground motion and the TCU102 forward-directivity ground motion. In addition, extensive damage to the isolation bearing under near-field ground motions indicates that the isolation bearings cannot be used in near-field conditions.

In the analysis, the differential effect of the ground motion is not considered, which may have a particular impact on the seismic response of a bridge. In addition, the study of near-field ground motion characteristics also needs to be further strengthened to better study its influence on the seismic response of a bridge.

## 6. Conclusions

This study created the damage constitutive models of steel and concrete material, the fiber beam-column element model, and the bearing model to establish a numerical analysis model of a bridge to study the effects of near-field (fling-step and forward-directivity ground motions) and far-field ground motions on isolated and nonisolated bridges. The following research results are obtained:

(1) The seismic responses of nonisolated bridges, such as girder acceleration, pier displacement, pier damage, and bearing displacement under fling-step ground motions and forward-directivity ground motions, increased to a certain extent compared to those under far-field ground motions. The pier displacement of the nonisolated bridges under forward-directivity ground motions is greater than that under fling-step ground motions, which also leads to more significant pier damage of the nonisolated bridges under forward-directivity ground motions.

(2) Isolation bearings can effectively reduce various seismic responses of a bridge (girder acceleration, pier displacement, pier shear force, and pier damage) under far-field ground motions. Isolation bearings can effectively isolate and protect the bridge. Under the TCU068 fling-step ground motions and TCU102 forward-directivity ground motions, the isolation bearings do not work and even amplify the seismic response of the bridge. However, the isolation bearings have an excellent isolation effect on the seismic response of bridges under most near-field ground motions. The isolation effect of isolation bearings under forward-directivity ground motion is better than that under fling-step ground motion.

(3) Compared with the far-field ground motions, the displacement of the isolation bearings under the fling-step ground motion and the forward-directivity ground motion is more extensive. This is the main reason for the damage to isolation bearings. Extensive damage to the isolation bearings under the near-field ground motions indicates that they cannot be directly used under near-field conditions.

(4) Under the near-field ground motions, nonisolated bridges often fail due to severe damage to the piers, while isolated bridges often fail due to the destruction of isolation bearings; sometimes, even the setting of the isolation bearings aggravates the seismic response of the bridges and leads to bridge failure. Under the far-field ground motions, the nonisolated bridge may not be seriously damaged, or the bridge may fail due to the severe damage to the piers. The setting of the isolation bearings can effectively reduce the response of the bridge and ensure the safety of the bridge.

Though the research results in this study cannot be directly applied in design practice, it was found that the isolation bearing may be damaged under near-field ground motions and cannot be directly implemented in practice, which needs further study. In addition, it was found that the failure modes of the isolated and nonisolated bridges under near-field ground motions were different, which provides an essential basis for the seismic design of bridges.

## Data Availability

The data used to support the findings of this study are available from the corresponding author upon request.

## Conflicts of Interest

The authors declare that there are no conflicts of interest regarding the publication of this paper.

## Acknowledgments

This research was funded by the National Natural Science Foundation of China (grant no. 52108481), the Scientific and Technological Innovation Programs of Higher Education Institutions in Shanxi (grant no. 2019L0547), and the Fundamental Research Program of Shanxi Province (grant nos. 201901D111134, 201901D111169, and 201801D221233).

## References

[1] J. Jia, X. Du, and Q. Han, "A state-of-the-art review of near-fault earthquake ground motion characteristics and effects on engineering structures," *Journal of Building Structures*, vol. 36, no. 1, pp. 1–12, 2015.

[2] Q. F. Liu, Y. F. Yuan, X. Jin, and H. P. Ding, "Basic characteristics of near-fault ground motion," *Earthquake Engineering and Engineering Variation*, vol. 26, no. 1, pp. 1–10, 2006.

[3] Y. Lu and M. Panagiotou, "Characterization and representation of near-fault ground motions using cumulative pulse extraction with wavelet analysis," *Bulletin of the Seismological Society of America*, vol. 104, no. 1, pp. 410–426, 2014.

[4] J. Zhong, T. Yang, Y. Pang, and W. Yuan, "A novel structure-pulse coupled model for quantifying the column ductility demand under pulse-like GMs," *Journal of Earthquake Engineering*, pp. 1–19, 2021.

[5] J. Zhong, L. Jiang, Y. Pang, and W. Yuan, "Near-fault seismic risk assessment of simply supported bridges," *Earthquake Spectra*, vol. 36, no. 4, pp. 1645–1669, 2020.

[6] M. H. Jónsson, B. Bessason, and E. Haflidason, "Earthquake response of a base-isolated bridge subjected to strong near-fault ground motion," *Soil Dynamics and Earthquake Engineering*, vol. 30, no. 6, pp. 447–455, 2010.

[7] H. Wei, Z. Lu, and Z. Wang, "Isolation characteristic analysis of simple supported bridge to near fault ground motions," *Journal of Tongji University*, vol. 38, no. 1, pp. 39–44, 2010.

[8] R. S. Jalali, M. B. Jokandan, and M. D. Trifunac, "Earthquake response of a three-span bridge, with mid-span supported by isolators, to near-field pulse and permanent-displacement step," *Soil Dynamics and Earthquake Engineering*, vol. 48, pp. 89–103, 2013.

[9] R. S. Jalali, M. Bahari Jokandan, and M. D. Trifunac, "Earthquake response of a three-span, simply supported bridge to near-field pulse and permanent-displacement step," *Soil Dynamics and Earthquake Engineering*, vol. 43, pp. 380–397, 2012.

[10] M. Ismail, J. Rodellar, and J. R. Casas, "Seismic behavior of RNC-isolated bridges: a comparative study under near-fault, long-period, and pulse-like ground motions," *Advances in Materials Science and Engineering*, vol. 2016, Article ID 1897045, 11 pages, 2016.

[11] D. Losanno, H. A. Hadad, and G. Serino, "Seismic behavior of isolated bridges with additional damping under far-field and near fault ground motion," *Earthquakes and Structures*, vol. 13, no. 2, pp. 119–130, 2017.

[12] W.-I. Liao, C.-H. Loh, and B.-H. Lee, "Comparison of dynamic response of isolated and non-isolated continuous girder bridges subjected to near-fault ground motions," *Engineering Structures*, vol. 26, no. 14, pp. 2173–2183, 2004.

[13] E. Kalkan and S. K. Kunnath, "Effects of fling step and forward directivity on seismic response of buildings," *Earthquake Spectra*, vol. 22, no. 2, pp. 367–390, 2006.

[14] W. Zheng, H. Wang, H. Hao, K. Bi, and H. Shen, "Performance of bridges isolated with sliding-lead rubber bearings subjected to near-fault earthquakes," *International Journal of Structural Stability and Dynamics*, vol. 20, no. 02, pp. 2050023–2050030, 2020.

[15] L. Jiang, J. Zhong, and W. Yuan, "The pulse effect on the isolation device optimization of simply supported bridges in near-fault regions," *Structures*, vol. 27, no. 6, pp. 853–867, 2020.

[16] I. Buckle, S. Nagarajaiah, and K. Ferrell, "Stability of elastomeric isolation bearings: experimental study," *Journal of Structural Engineering*, vol. 128, no. 1, pp. 3–11, 2002.

[17] Z. X. Li, Y. Gao, and N. Li, "RSAPS-based isolation element model," *Engineering Mechanics*, vol. 33, no. 4, pp. 144–149, 2016.

[18] J. Zhong, M. Ni, H. Hu, W. Yuan, H. Yuan, and Y. Pang, "Uncoupled multivariate power models for estimating performance-based seismic damage states of column curvature ductility," *Structures*, vol. 36, pp. 752–764, 2022.

[19] W. Wang, F. Zhou, and J. Zhong, "An efficient axial-flexure-shear fiber beam model for dynamic analyses of beam-column framed structural systems under impact loading," *Ocean Engineering*, vol. 245, Article ID 110349, 2022.

[20] Y. A. Heo and S. K. Kunnath, "Damage-based seismic performance evaluation of reinforced concrete frames," *International Journal of Concrete Structures and Materials*, vol. 7, no. 3, pp. 175–182, 2013.

[21] Z. X. Li, Y. Chen, and N. Li, "A Damage model for reinforced concrete members based on material damage," *Engineering Mechanics*, vol. 31, no. 6, pp. 53–59, 2014.

[22] Y. Gao, Z. X. Li, and N. Li, "Damage analysis of reinforced concrete members based on RSAPS," *Journal of Tianjin University*, vol. 50, no. 4, pp. 345–350, 2017.

[23] Z. Li and G. D. Hatzigeorgiou, "Seismic damage analysis of RC structures using fiber beam-column elements," *Soil Dynamics and Earthquake Engineering*, vol. 32, no. 1, pp. 103–110, 2012.

[24] Y. Gao, *Study On RSAPS Based Refined Simulation Models for Seismic Damage Analysis of RC Bridge Components*, PhD Thesis, Tianjin University, Tianjin, China, 2016.

[25] J. Chen, "Seismic Response Analysis and Isolation Effect of RC Frame Structure under Multi-Dimensional Near-Field Earthquake," Master Thesis, North University of China, Taiyuan, China, 2021.

[26] R. Sehhati, A. Rodriguez-Marek, M. Elgawady, and W. F. Cofer, "Effects of near-fault ground motions and equivalent pulses on multi-story structures," *Engineering Structures*, vol. 33, no. 3, pp. 767–779, 2011.
[27] H. Moniri, "Evaluation of seismic performance of reinforced concrete (RC) buildings under near-field earthquakes," *International Journal of Advanced Structural Engineering*, vol. 9, no. 1, pp. 13–25, 2017.
[28] X. Z. Li, L. Xin, M. Liu, S. Y. Dai, and L. Xiao, "Effect of near-fault fling-step motions on a five-span two-frame bridge," *Earthquake Engineering and Engineering Dynamics*, vol. 39, no. 2, pp. 169–176, 2019.
[29] S. Z. Wang and G. L. Bai, "Study on IDA of high-rise frame-shear wall structure under near-fault fling-step-type ground motion," *Journal of Disaster Prevention and Mitigation Engineering*, vol. 39, no. 3, pp. 437–444, 2019.
[30] P. Earthquake Engineering Research Center (Peer), *PEER strong Motion Database*, University of California, Berkeley, CA, USA, 2000.
[31] M. H. Mohd-Yassin, *Nonlinear Analysis of Pressured concrete Structures under Monotonic and Cyclic Loads*, PhD Thesis, University of California, Berkeley, CA, USA, 1994.
[32] J. Yue, J. Qian, and D. E. Beskos, "A generalized multi-level seismic damage model for RC framed structures," *Soil Dynamics and Earthquake Engineering*, vol. 80, pp. 25–39, 2016.
[33] M. Menegotto and P. E. Pinto, "Slender RC compressed members in biaxial bending," *Journal of the Structural Division*, vol. 103, no. 3, pp. 587–605, 1977.
[34] F. C. Filippou, E. P. Popov, and V. V. Bertero, "Effects of Bond Determination on Hysterical Behavior of Reinforced concrete Joins," EERC Report 83/19, Earthquake Engineering Research Center University of California, Berkeley, CA, USA, 1983.
[35] N. Bonora, "A nonlinear CDM model for ductile failure," *Engineering Fracture Mechanics*, vol. 58, no. 1-2, pp. 11–28, 1997.
[36] A. Pirondi and N. Bonora, "Modeling ductile damage under fully reversed cycling," *Computational Materials Science*, vol. 26, pp. 129–141, 2003.
[37] F. Casciati, "Stochastic dynamics of hysteretic media," *Structural Safety*, vol. 6, no. 2-4, pp. 259–269, 1989.
[38] J. Weisman and G. P. Warn, "Stability of elastomeric and lead-rubber seismic isolation bearings," *Journal of Structural Engineering*, vol. 138, no. 2, pp. 215–223, 2012.
[39] Ministry of Construction of the People's Republic of China, *Code for Design of Concrete Structures (GB 50010-2010)*, China Architecture and Building Press, Beijing, China, 2010.